

MURA Dataset: Towards Radiologist-Level Abnormality Detection in Musculoskeletal Radiographs

Pranav Rajpurkar^{*1} Jeremy Irvin^{*1} Aarti Bagul¹ Daisy Ding¹ Tony Duan¹
 Hershel Mehta¹ Brandon Yang¹ Kaylie Zhu¹ Dillon Laird¹ Robyn L. Ball²
 Curtis Langlotz³ Katie Shpanskaya³ Matthew P. Lungren³ Andrew Ng¹

Abstract

We introduce MURA, a large dataset of musculoskeletal radiographs containing 40,895 images from 14,982 studies, where each study is manually labeled by radiologists as either normal or abnormal. On this dataset, we train a 169-layer densely connected convolutional network to detect and localize abnormalities. To evaluate our model robustly and to get an estimate of radiologist performance, we collect additional labels from board-certified Stanford radiologists on the test set, consisting of 209 musculoskeletal studies. We compared our model and radiologists on the Cohen's kappa statistic, which expresses the agreement of our model and of each radiologist with the gold standard, defined as the majority vote of a disjoint group of radiologists. We find that our model achieves performance comparable to that of radiologists. Model performance is higher than the best radiologist performance in detecting abnormalities on finger studies and equivalent on wrist studies. However, model performance is lower than best radiologist performance in detecting abnormalities on elbow, forearm, hand, humerus, and shoulder studies, indicating that the task is a good challenge for future research. To encourage advances, we have made our dataset freely available at <https://stanfordmlgroup.github.io/projects/mura>.

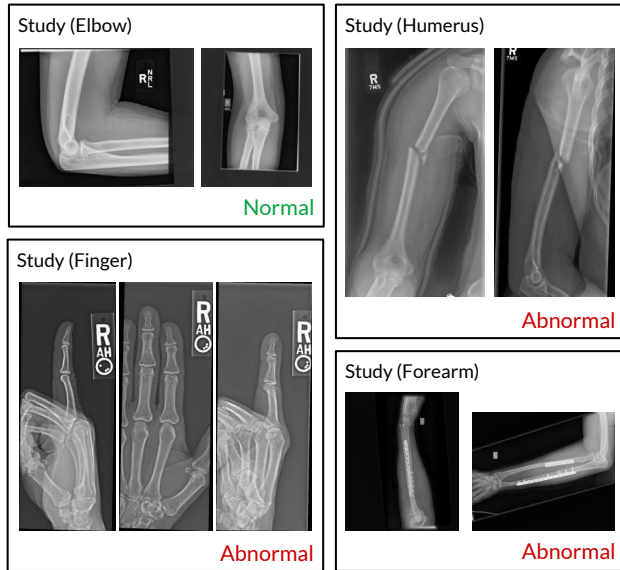


Figure 1. The MURA dataset contains 14,982 musculoskeletal studies of the upper extremity, where each study contains one or more views and is manually labeled by radiologists as either normal or abnormal. These examples show a normal elbow study (top left), an abnormal humerus study with a fracture (top right), an abnormal finger study with degenerative changes (bottom left), and an abnormal forearm study (bottom right) demonstrating operative plate and screw fixation of radial and ulnar fractures.

1. Introduction

Large, high-quality datasets have played a critical role in driving progress of fields with deep learning methods (Deng et al., 2009). To this end, we introduce MURA, a large dataset of radiographs, containing 14,982 musculoskeletal studies of the upper extremity. Each study contains one or more views (images) and is manually labeled by radiologists as either normal or abnormal.

The abnormality detection task, or in other words determining whether a radiographic study is normal or

^{*}Equal contribution ¹Stanford University Department of Computer Science ²Stanford University Department of Medicine ³Stanford University Department of Radiology. Correspondence to: Pranav Rajpurkar <pranavsr@cs.stanford.edu>, Jeremy Irvin <jirvin16@cs.stanford.edu>.

Study	Normal	Abnormal	Total
Elbow	1,203	768	1,971
Finger	1,389	753	2,142
Forearm	677	380	1,057
Hand	1,613	602	2,215
Humerus	411	367	778
Shoulder	1,479	1,594	3,073
Wrist	2,295	1,451	3,746
Total	9,067	5,915	14,982

Table 1. MURA contains 9,067 normal and 5,915 abnormal musculoskeletal radiographic studies of the upper extremity including the shoulder, humerus, elbow, forearm, wrist, hand, and finger. MURA is one of the largest public radiographic image datasets.

abnormal, is a critical radiological task: a study interpreted as normal rules out disease and can eliminate the need for patients to undergo further diagnostic procedures or interventions. Musculoskeletal conditions affect more than 1.7 billion people worldwide (BMU, 2017), and are the most common cause of severe, long-term pain and disability (Woolf & Pfleger, 2003), with 30 million emergency department visits annually and increasing. Our dataset, MURA, contains 9,067 normal and 5,915 abnormal musculoskeletal radiographic studies of the upper extremity including the shoulder, humerus, elbow, forearm, wrist, hand, and finger. MURA is one of the largest public radiographic image datasets.

On MURA, we developed a competitive abnormality detection model. The model takes as input one or more views for a study of an upper extremity. On each view, a 169-layer convolutional neural network predicts the probability of abnormality; the per-view probabilities are then averaged to output the probability of abnormality for the study.

To evaluate models robustly and to get an estimate of radiologist performance, we collected six additional labels from board-certified radiologists on a holdout test set of 209 studies. We compare the performance of our model and radiologists, and find that our model achieves performance comparable to that of radiologists. Model performance is higher than the best radiologist’s performance in detecting abnormalities on finger studies, and equivalent in wrist studies. However, model performance is lower than best radiologist’s performance in detecting abnormalities on elbow, forearm, hand, humerus, and shoulder studies. We have made our dataset freely available to encourage advances in medical imaging models.

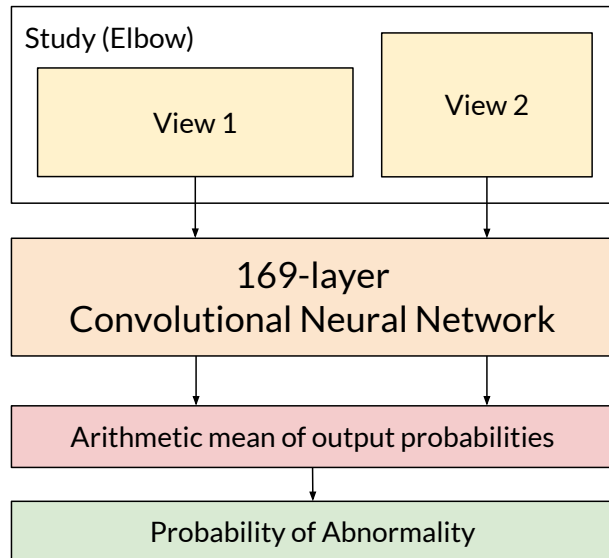


Figure 2. The model takes as input one or more views for a study. On each view, our 169-layer convolutional neural network predicts the probability of abnormality; the per-view probabilities are then averaged to output the probability of abnormality for the study.

2. MURA

The MURA abnormality detection task is a binary classification task, where the input is an upper extremity radiograph study — with each study containing one or more views (images) — and the expected output is a binary label $y \in \{0, 1\}$ indicating whether the study is normal or abnormal, respectively.

2.1. Data Collection

Our institutional review board approved study collected de-identified, HIPAA-compliant images from the Picture Archive and Communication System (PACS) of Stanford Hospital. We assembled a dataset of musculoskeletal radiographs consisting of 14,982 studies from 12,251 patients, with a total of 40,895 multi-view radiographic images. Each belongs to one of seven standard upper extremity radiographic study types: elbow, finger, forearm, hand, humerus, shoulder, and wrist. Table 1 summarizes the distribution of normal and abnormal studies.

Each study was manually labeled as normal or abnormal by board-certified radiologists from the Stanford Hospital at the time of clinical radiographic interpretation in the diagnostic radiology environment between 2001 and 2012. The labeling was performed during interpretation on DICOM images presented on at least 3 megapixel PACS medical grade display with max

	Radiologist 1	Radiologist 2	Radiologist 3	Model
Elbow	0.795 (0.770, 0.819)	0.733 (0.703, 0.764)	0.738 (0.709, 0.767)	0.733 (0.703, 0.764)
Finger	0.304 (0.249, 0.358)	0.403 (0.339, 0.467)	0.410 (0.358, 0.463)	0.525 (0.476, 0.573)
Forearm	0.796 (0.772, 0.821)	0.802 (0.779, 0.825)	0.798 (0.774, 0.822)	0.670 (0.634, 0.705)
Hand	0.661 (0.623, 0.698)	0.927 (0.917, 0.937)	0.789 (0.762, 0.815)	0.780 (0.752, 0.809)
Humerus	0.867 (0.850, 0.883)	0.733 (0.703, 0.764)	0.933 (0.925, 0.942)	0.800 (0.776, 0.824)
Shoulder	0.864 (0.847, 0.881)	0.791 (0.765, 0.816)	0.864 (0.847, 0.881)	0.795 (0.770, 0.819)
Wrist	0.791 (0.766, 0.817)	0.931 (0.922, 0.940)	0.931 (0.922, 0.940)	0.931 (0.922, 0.940)
Overall	0.724 (0.719, 0.728)	0.766 (0.762, 0.770)	0.780 (0.777, 0.784)	0.749 (0.744, 0.753)

Table 2. We compare radiologists and our model on the Cohen’s kappa statistic, which expresses the agreement of each radiologist/model with the gold standard, defined as the majority vote of a disjoint group of radiologists. We highlight the best (green) and worst (red) performances on each of the study types and in aggregate. On finger studies, model performance is significantly higher than the best radiologist performance. On wrist studies, model performance is equivalent to the best radiologist performance. On hand, humerus, and shoulder studies, model performance is higher than the worst radiologist performance but lower than the best radiologist performance. On elbow and shoulder studies, model performance is comparable to the worst radiologist performance. On forearm studies, model performance is significantly worse than the worst radiologist performance.

luminance 400 cd/m^2 and min luminance 1 cd/m^2 with pixel size of 0.2 and native resolution of 1500 x 2000 pixels. The clinical images vary in resolution and in aspect ratios. We split the dataset into training (11,255 patients, 13,565 studies, 37,111 images), validation (788 patients, 1,208 studies, 3,225 images), and test (208 patients, 209 studies, 559 images) sets. There is no overlap in patients between any of the sets.

2.2. Test Set Collection

To evaluate models and get a robust estimate of radiologist performance, we collected additional labels from board-certified Stanford radiologists on the test set, consisting of 209 musculoskeletal studies. The radiologists individually retrospectively reviewed and labeled each study in the test set as a DICOM file as normal or abnormal in the clinical reading room environment using the PACS system. The radiologists have 8.83 years of experience on average ranging from 2 to 25 years. The radiologists did not have access to any clinical information. Labels were entered into a standardized data entry program.

2.3. Abnormality Analysis

To investigate the types of abnormalities present in the dataset, we reviewed the radiologist reports to manually label 100 abnormal studies with the abnormality finding: 53 studies were labeled with fractures, 48 with hardware, 35 with degenerative joint diseases, and 29 with other miscellaneous abnormalities, including lesions and subluxations.

3. Model

The model takes as input one or more views for a study of an upper extremity. On each view, our 169-layer convolutional neural network predicts the probability of abnormality. We compute the overall probability of abnormality for the study by taking the arithmetic mean of the abnormality probabilities output by the network for each image. The model makes the binary prediction of abnormal if the probability of abnormality for the study is greater than 0.5. Figure 2 illustrates the model’s prediction pipeline.

3.1. Network Architecture and Training

We used a 169-layer convolutional neural network to predict the probability of abnormality for each image in a study. The network uses a Dense Convolutional Network architecture – detailed in Huang et al. (2016) – which connects each layer to every other layer in a feed-forward fashion to make the optimization of deep networks tractable. We replaced the final fully connected layer with one that has a single output, after which we applied a sigmoid nonlinearity.

For each image X of study type T in the training set, we optimized the weighted binary cross entropy loss

$$\begin{aligned} L(X, y) = & -w_{T,1} \cdot y \log p(Y = 1|X) \\ & -w_{T,0} \cdot (1 - y) \log p(Y = 0|X), \end{aligned}$$

where y is the label of the study, $p(Y = i|X)$ is the probability that the network assigns to the label i , $w_{T,1} = |N_T|/(|A_T| + |N_T|)$, and $w_{T,0} = |A_T|/(|A_T| +$

Dataset	Study Type	Label	Images
MURA	Musculoskeletal (Upper Extremity)	Abnormality	41,299
Pediatric Bone Age (AIMI)	Musculoskeletal (Hand)	Bone Age	14,236
0.E.1 (OAI)	Musculoskeletal (Knee)	K&L Grade	8,892
Digital Hand Atlas (Gertych et al., 2007)	Musculoskeletal (Left Hand)	Bone Age	1,390
ChestX-ray14 (Wang et al., 2017)	Chest	Multiple Pathologies	112,120
OpenI (Demner-Fushman et al., 2015)	Chest	Multiple Pathologies	7,470
MC (Jaeger et al., 2014)	Chest	Abnormality	138
Shenzhen (Jaeger et al., 2014)	Chest	Tuberculosis	662
JSRT (Shiraishi et al., 2000)	Chest	Pulmonary Nodule	247
DDSM (Heath et al., 2000)	Mammogram	Breast Cancer	10,239

Table 3. Overview of publicly available medical radiographic image datasets.

$|N_T|$) where $|A_T|$ and $|N_T|$ are the number of abnormal images and normal images of study type T in the training set, respectively.

Before feeding images into the network, we normalized each image to have the same mean and standard deviation of images in the ImageNet training set. We then scaled the variable-sized images to 224×224 . We augmented the data during training by applying random lateral inversions and rotations.

The weights of the network were initialized with weights from a model pretrained on ImageNet ([Deng et al., 2009](#)). The network was trained end-to-end using Adam with default parameters $\beta_1 = 0.9$ and $\beta_2 = 0.999$ ([Kingma & Ba, 2014](#)). We trained the model using minibatches of size 8. We used an initial learning rate of 0.0001 that is decayed by a factor of 10 each time the validation loss plateaus after an epoch, and chose the model with the lowest validation loss.

4. Radiologist vs. Model Performance

We assessed the performance of both radiologists and our model on the test set. Recall that for each study in the test set, we collected additional normal/abnormal labels from 6 board-certified radiologists. We randomly chose 3 of these radiologists to create a gold standard, defined as the majority vote of labels of the

radiologists. We used the other 3 radiologists to get estimates of radiologist performance on the task.

We compared radiologists and our model on the Cohen's kappa statistic (κ), which expresses the agreement of each radiologist/model with the gold standard. We also reported the 95% confidence interval using the standard error of kappa ([McHugh, 2012](#)). Table 2 summarizes the performance of both radiologists and the model on the different study types and in aggregate. The radiologists achieved their highest performance on either wrist studies (radiologist 2) or humerus studies (radiologists 1 and 3), and their lowest performance on finger studies. The model also achieved its highest performance on wrist studies and its lowest performance on finger studies.

We compared the best radiologist performance on each of the study types against model performance. On finger studies, the model performance of 0.525 (95% CI 0.476, 0.573) was significantly higher than the best radiologist performance of 0.410 (95% CI 0.358, 0.463). On wrist studies, the model performance of 0.931 (95% CI 0.922, 0.940) was equivalent to the best radiologist's performance. On all other study types, and overall, model performance was significantly lower than best radiologist's performance.

We also compared the worst radiologist performance on each of the study types against model performance.



(a) Three views of the right wrist in a patient with distal radius and ulna fractures after casting. The model predicted the probability of abnormality in each view to be greater than 99%, correctly predicting the study as abnormal.

(b) Two radiographic views of the finger in a patient with a prior fifth proximal phalynx fracture status post screw and plate fixation. The model predicted the probability of abnormality in both views to be greater than 99.9%, correctly predicting the study as abnormal.

Figure 3. Our model localizes abnormalities it identifies using Class Activation Maps, which highlight the areas of the radiograph that are most important for making the prediction of abnormality.

On forearm studies, the model performance of 0.670 (95% CI 0.634, 0.705) was significantly lower than the worst radiologist’s performance of 0.796 (95% CI 0.772, 0.821). On elbow studies, the model performance of 0.733 (95% CI 0.703, 0.764) was not significantly different than the worst radiologist’s performance of 0.733 (95% CI 0.703, 0.764). On all other study types, and overall, model performance was higher than the worst radiologist performance, and significantly so except on shoulder studies.

5. Model Interpretation

We visualize the parts of the radiograph which contribute most to the model’s prediction of abnormality by using class activation mappings (CAMs) (Zhou et al., 2016). We input the radiograph X into the fully trained network to obtain the feature maps output by the final convolutional layer. To compute the CAM $M(X)$, we take a weighted average of the feature maps using the weights of the final fully connected layer. Denote the k th feature map output by the network on image X by $f_k(X)$ and the k th fully connected weight by w_k . Formally,

$$M(X) = \sum_k w_k f_k(X).$$

To highlight the salient features in the original radiograph which contribute the most to the network predictions, we upscale the CAM $M(X)$ to the dimensions of the image and overlay the image. We provide several examples of CAMs along with radiologist commentary in Figure 3.

6. Related Work

Large datasets have led to deep learning algorithms achieving or approaching human-level performance on tasks such as image recognition (Deng et al., 2009), speech recognition (Hannun et al., 2014), and question answering (Rajpurkar et al., 2016). Large medical datasets have led to expert-level performance on detection of diabetic retinopathy (Gulshan et al., 2016), skin cancer (Esteva et al., 2017), heart arrhythmias (Rajpurkar et al., 2017a), brain hemorrhage (Grewal et al., 2017), pneumonia (Rajpurkar et al., 2017b), and hip fractures (Gale et al., 2017).

There has been a growing effort to make repositories of medical radiographs openly available. Table 3 provides a summary of the publicly available datasets of medical radiographic images. Previous datasets are smaller than MURA in size, with the exception of the recently released ChestX-ray14 (Wang et al., 2017), which contains 112,120 frontal-view chest radiographs with up

to 14 thoracic pathology labels. However, their labels were not provided directly from a radiologist, but instead automatically generated from radiologists' text reports.

There are few openly available musculoskeletal radiograph databases. The Stanford Program for Artificial Intelligence in Medicine and Imaging hosts a dataset containing pediatric hand radiographs annotated with skeletal age (AIMI). The Digital Hand Atlas consists of left hand radiographs from children of various ages labeled with radiologist readings of bone age (Gertych et al., 2007). The OsteoArthritis Initiative hosts the O.E.1 dataset which contains knee radiographs labeled with the K&L grade of osteoarthritis (OAI). Each of these datasets contain less than 15,000 images.

7. Discussion

Abnormality detection in musculoskeletal radiographs has important clinical applications. First, an abnormality detection model could be utilized for worklist prioritization. In this scenario, the studies detected as abnormal could be moved ahead in the image interpretation workflow, allowing the sickest patients to receive quicker diagnoses and treatment. Furthermore, the examinations identified as normal could be automatically assigned a preliminary reading of "normal"; this could mean (1) normal examinations can be properly triaged as lower priority on a worklist (2) more rapid results can be conveyed to the ordering provider (and patient) which could improve disposition in other areas of the healthcare system (i.e., discharged from the ED more quickly) (3) a radiology report template for the normal study could be served to the interpreting radiologist for more rapid review and approval.

Second, automated abnormality localization could help combat radiologist fatigue. Radiologists all over the world are reading an increasing number of cases with more images per case. Physician shortages exacerbate the problem, especially for radiologists in medically underserved areas (Nakajima et al., 2008). While physician fatigue is a common problem that affects all healthcare professionals, radiologists are particularly susceptible, and there is evidence that workloads are so demanding that fatigue may impact diagnostic accuracy. (Bhargavan & Sunshine, 2005; Lu et al., 2008; Berlin, 2000; Fitzgerald, 2001). A study examining radiologist fatigue in the interpretation of musculoskeletal radiographs found a statistically significant decrease in fracture detection at the end of the work day compared to beginning of work day (Krupinski et al., 2010). Thus, a model which can perform automatic abnormality localization could highlight the

portion of the image that is recognized as abnormal by the model, drawing the attention of the clinician. If effective, this could lead to more efficient interpretation of the imaging examination, reduce errors, and help standardize quality. More studies are necessary to evaluate the optimal integration of this model and other deep learning models in the clinical setting.

8. Acknowledgements

We would like to acknowledge the Stanford Program for Artificial Intelligence in Medicine and Imaging for clinical dataset infrastructure support (AIMI.stanford.edu).

References

- 2017. URL <http://www.boneandjointburden.org/2014-report>.
- AIMI. Artificial intelligence in medicine & imaging: Available labeled medical datasets. <https://aimi.stanford.edu/available-labeled-medical-datasets>. [Online; accessed 2-December-2017].
- Berlin, Leonard. Liability of interpreting too many radiographs. *American Journal of Roentgenology*, 175(1):17–22, 2000.
- Bhargavan, Mythreyi and Sunshine, Jonathan H. Utilization of radiology services in the united states: levels and trends in modalities, regions, and populations. *Radiology*, 234(3):824–832, 2005.
- Demner-Fushman, Dina, Kohli, Marc D, Rosenman, Marc B, Shooshan, Sonya E, Rodriguez, Laritza, Antani, Sameer, Thoma, George R, and McDonald, Clement J. Preparing a collection of radiology examinations for distribution and retrieval. *Journal of the American Medical Informatics Association*, 23(2):304–310, 2015.
- Deng, Jia, Dong, Wei, Socher, Richard, Li, Li-Jia, Li, Kai, and Fei-Fei, Li. Imagenet: A large-scale hierarchical image database. In *Computer Vision and Pattern Recognition, 2009. CVPR 2009. IEEE Conference on*, pp. 248–255. IEEE, 2009.
- Esteva, Andre, Kuprel, Brett, Novoa, Roberto A, Ko, Justin, Swetter, Susan M, Blau, Helen M, and Thrun, Sebastian. Dermatologist-level classification of skin cancer with deep neural networks. *Nature*, 542(7639):115–118, 2017.
- Fitzgerald, Richard. Error in radiology. *Clinical radiology*, 56(12):938–946, 2001.

Gale, W., Oakden-Rayner, L., Carneiro, G., Bradley, A. P., and Palmer, L. J. Detecting hip fractures with radiologist-level performance using deep neural networks. *ArXiv e-prints*, November 2017.

Gertych, Arkadiusz, Zhang, Aifeng, Sayre, James, Pospiech-Kurkowska, Sylwia, and Huang, HK. Bone age assessment of children using a digital hand atlas. *Computerized Medical Imaging and Graphics*, 31(4):322–331, 2007.

Grewal, Monika, Srivastava, Muktabh Mayank, Kumar, Pukit, and Varadarajan, Srikrishna. Radnet: Radiologist level accuracy using deep learning for hemorrhage detection in ct scans. *arXiv preprint arXiv:1710.04934*, 2017.

Gulshan, Varun, Peng, Lily, Coram, Marc, Stumpe, Martin C, Wu, Derek, Narayanaswamy, Arunachalam, Venugopalan, Subhashini, Widner, Kasumi, Madams, Tom, Cuadros, Jorge, et al. Development and validation of a deep learning algorithm for detection of diabetic retinopathy in retinal fundus photographs. *Jama*, 316(22):2402–2410, 2016.

Hannun, Awni, Case, Carl, Casper, Jared, Catanzaro, Bryan, Diamos, Greg, Elsen, Erich, Prenger, Ryan, Satheesh, Sanjeev, Sengupta, Shubho, Coates, Adam, et al. Deep speech: Scaling up end-to-end speech recognition. *arXiv preprint arXiv:1412.5567*, 2014.

Heath, Michael, Bowyer, Kevin, Kopans, Daniel, Moore, Richard, and Kegelmeyer, W Philip. The digital database for screening mammography. In *Proceedings of the 5th international workshop on digital mammography*, pp. 212–218. Medical Physics Publishing, 2000.

Huang, Gao, Liu, Zhuang, Weinberger, Kilian Q, and van der Maaten, Laurens. Densely connected convolutional networks. *arXiv preprint arXiv:1608.06993*, 2016.

Jaeger, Stefan, Candemir, Sema, Antani, Sameer, Wang, Yi-Xiang J, Lu, Pu-Xuan, and Thoma, George. Two public chest x-ray datasets for computer-aided screening of pulmonary diseases. *Quantitative imaging in medicine and surgery*, 4(6):475, 2014.

Kingma, Diederik and Ba, Jimmy. Adam: A method for stochastic optimization. *arXiv preprint arXiv:1412.6980*, 2014.

Krupinski, Elizabeth A, Berbaum, Kevin S, Caldwell, Robert T, Schartz, Kevin M, and Kim, John. Long radiology workdays reduce detection and accommodation accuracy. *Journal of the American College of Radiology*, 7(9):698–704, 2010.

Lu, Ying, Zhao, Shoujun, Chu, Philip W, and Arenson, Ronald L. An update survey of academic radiologists' clinical productivity. *Journal of the American College of Radiology*, 5(7):817–826, 2008.

McHugh, Mary L. Interrater reliability: the kappa statistic. *Biochemia Medica*, 22(3):276–282, October 2012. ISSN 1330-0962. URL <https://www.ncbi.nlm.nih.gov/pmc/articles/PMC3900052/>.

Nakajima, Yasuo, Yamada, Kei, Imamura, Keiko, and Kobayashi, Kazuko. Radiologist supply and workload: international comparison. *Radiation medicine*, 26(8):455–465, 2008.

OAI. Osteoarthritis initiative: a multi-center observational study of men and women. <https://oai.epi-ucsf.org/datarelease/>. [Online; accessed 2-December-2017].

Rajpurkar, Pranav, Zhang, Jian, Lopyrev, Konstantin, and Liang, Percy. Squad: 100,000+ questions for machine comprehension of text. *arXiv preprint arXiv:1606.05250*, 2016.

Rajpurkar, Pranav, Hannun, Awni Y, Haghpanahi, Masoumeh, Bourn, Codie, and Ng, Andrew Y. Cardiologist-level arrhythmia detection with convolutional neural networks. *arXiv preprint arXiv:1707.01836*, 2017a.

Rajpurkar, Pranav, Irvin, Jeremy, Zhu, Kaylie, Yang, Brandon, Mehta, Hershel, Duan, Tony, Ding, Daisy, Bagul, Aarti, Langlotz, Curtis, Shpanskaya, Katie, et al. Chexnet: Radiologist-level pneumonia detection on chest x-rays with deep learning. *arXiv preprint arXiv:1711.05225*, 2017b.

Shiraishi, Junji, Katsuragawa, Shigehiko, Ikezoe, Junpei, Matsumoto, Tsuneo, Kobayashi, Takeshi, Komatsu, Ken-ichi, Matsui, Mitate, Fujita, Hiroshi, Kodera, Yoshie, and Doi, Kunio. Development of a digital image database for chest radiographs with and without a lung nodule: receiver operating characteristic analysis of radiologists' detection of pulmonary nodules. *American Journal of Roentgenology*, 174(1):71–74, 2000.

Wang, Xiaosong, Peng, Yifan, Lu, Le, Lu, Zhiyong, Bagheri, Mohammadhadi, and Summers, Ronald M. Chestx-ray8: Hospital-scale chest x-ray database and benchmarks on weakly-supervised classification and localization of common thorax diseases. *arXiv preprint arXiv:1705.02315*, 2017.

Woolf, Anthony D and Pfleger, Bruce. Burden of major musculoskeletal conditions. *Bulletin of the World Health Organization*, 81(9):646–656, 2003.

Zhou, Bolei, Khosla, Aditya, Lapedriza, Agata, Oliva, Aude, and Torralba, Antonio. Learning deep features for discriminative localization. In *Proceedings of the IEEE Conference on Computer Vision and Pattern Recognition*, pp. 2921–2929, 2016.